Neurosci. Bull. February, 2017, 33(1):1–16
DOI 10.1007/s12264-016-0086-x

www.neurosci.cn
www.springer.com/12264

ORIGINAL ARTICLE

Expression of Phospho-MeCP2s in the Developing Rat Brain and Function of Postnatal MeCP2 in Cerebellar Neural Cell Development

Fang Liu[1] · Jing-Jing Ni[1] · Feng-Yan Sun[1,2]

Received: 20 May 2016 / Accepted: 2 November 2016 / Published online: 19 December 2016

Abstract Abnormal expression and dysfunction of methyl-CpG binding protein 2 (MeCP2) cause Rett syndrome (RTT). The diverse phosphorylation modifications modulate MeCP2 function in neural cells. Using western blot and immunohistochemistry, we examined the expression patterns of MeCP2 and three phospho-MeCP2s (pMeCP2s) in the developing rat brain. The expression of MeCP2 and phospho-S80 (pS80) MeCP2 increased while pS421 MeCP2 and pS292 MeCP2 decreased with brain maturation. In contrast to the nuclear localization of MeCP2 and pS80 MeCP2, pS421 MeCP2 and pS292 MeCP2 were mainly expressed in the cytoplasmic compartment. Apart from their distribution in neurons, they were also detected at a low level in astrocytes. Postnatally-initiated MeCP2 deficiency affected cerebellar neural cell development, as determined by the abnormal expression of GFAP, DCX, Tuj1, MAP-2, and calbindin-D28k. Together, these results demonstrate that MeCP2 and diverse pMeCP2s have distinct features of spatio-temporal expression in the rat brain, and that the precise levels of MeCP2 in the postnatal period are vital to cerebellar neural cell development.

Keywords MeCP2 · Phospho-MeCP2 · Brain development · Cytoplasm · Astrocyte · Cerebellum

Introduction

Methyl-CpG binding protein 2 (MeCP2) is a crucial epigenetic modulator in the mammalian brain. It functions as a transcriptional repressor or activator *via* binding to methylated CpGs in the promoters and nearby regions of target genes [1]. Recent studies have shown that phosphorylation has extremely important effects on the modulation of MeCP2 function [2]. Activity-dependent phosphorylation of MeCP2 at serine 421 (S421) causes its separation from the promoter of *Bdnf* and increases the expression of BDNF in neurons [3]. In contrast, phospho-S80 is established under resting conditions in neurons and promotes the binding of MeCP2 to the promoters of target genes to repress gene transcription [4]. Strikingly, other studies have further shown that the transcriptional roles of pS421 MeCP2 and pS80 MeCP2 vary according to their specific target genes, and that pS421 MeCP2 can even bind across the genome without selectivity [4–6]. These findings illustrate the diversity and complexity of the functions of post-translational modifications of MeCP2 [7]. In a recent study, we showed that the expression of pS292 MeCP2, a newly-reported phospho-MeCP2 (pMeCP2), is induced in reactive astrocytes in the ischemic adult brain [8], but its function is not yet clear. Notably, diverse pMeCP2s can interact with distinct co-factors to initiate disparate transcriptional pathways [9], indicating that the dynamic balance between phosphorylation and dephosphorylation is crucial for MeCP2 function. However, although the characteristics of MeCP2 expression have been investigated, the developmental expression of pMeCP2s has not

Electronic supplementary material The online version of this article (doi:10.1007/s12264-016-0086-x) contains supplementary material, which is available to authorized users.

✉ Feng-Yan Sun
fysun@shmu.edu.cn

[1] Department of Neurobiology, Institute of Biomedical Sciences, State Key Laboratory of Medical Neurobiology, Shanghai Medical College, Fudan University, Shanghai 200032, China

[2] Research Center on Aging and Medicine, Shanghai Medical College, Fudan University, Shanghai 200032, China

attracted much attention. In view of this, a comprehensive understanding of the expression and distribution patterns of diverse pMeCP2s would be of great value.

MeCP2 is detectable in most tissues but is enriched in the brain [3]. It increases with brain development and is primarily expressed in mature neurons [10]. Recently, some studies have further reported the expression of MeCP2 in glial cells including astrocytes, oligodendrocytes, and microglia [11, 12]. Importantly, MeCP2-deficient astrocytes isolated from *Mecp2*$^{-/y}$ mice cannot support neuronal dendritic growth, indicating a critical role of MeCP2 in glial function [11]. However, to date, most studies have reported pMeCP2s exclusively in neurons [4, 5], except for the observation of astrocytic pS292 MeCP2 in our recent study [8]. Therefore, in this study we set out to identify the phenotypes of cells expressing pS80 MeCP2, pS421 MeCP2, and pS292 MeCP2 in the developing rat brain. As to intracellular localization, MeCP2 occurs predominantly in the nucleus, but it can be also expressed in the cytoplasm and postsynaptic compartment at a relatively low level [13, 14]. However, so far, most pMeCP2s have been observed mainly in the nucleus [6, 9], except for the cytoplasmic pS421 MeCP2 and pS292 MeCP2 reported in several studies [8, 15]. Hence, we also investigated the intracellular localization of pMeCP2s in the rat brain to assist further understanding of MeCP2 function.

The precise levels of MeCP2 are vital for brain development. Its abnormal expression causes Rett syndrome (RTT), a genetic neurological disorder [16]. Patients with RTT show normal development in the perinatal and early postnatal periods from 6 to 18 months, but exhibit symptoms thereafter, including the loss of speech, motor skills, and purposeful hand motions [17–19]. Effective clinical therapies remain limited, and the exact role of MeCP2 in the progression of the motor defects is unclear. At present, a variety of *Mecp2*-manipulated mouse models have been developed to investigate the function of MeCP2 in the brain [20]. It has been reported that both *Mecp2*-null and *Mecp2* transgenic mice acquire neurological phenotypes of RTT [21, 22], consistent with clinical observations. Notably, restoring the protein levels to normal in *Mecp2*-null or duplication mice rescues their neurological abnormalities [23]. These findings suggest that the disorders derived from deregulation of MeCP2 are reversible and raise possibilities for the treatment of MeCP2-related diseases. In addition, considering the delay in the phenotypic onset of RTT caused by germline *Mecp2* mutations and the pattern of MeCP2 expression, it is of great value to explore the function of MeCP2 in the postnatal brain. It has been shown that deletion of *MeCP2* after birth produces phenotypes comparable to those in *Mecp2*-null mice and disturbs mature neuronal networks as well as the expression of synaptic proteins [24, 25]. These findings indicate the requirement of MeCP2 to maintain brain functions in the postnatal period. Nevertheless, few studies have investigated its function in the postnatal cerebellum, which may offer a novel interpretation to the progression of the motor deficits in RTT patients. Therefore, we aimed to investigate the potential functions of MeCP2 in neural cell development in the postnatal cerebellum.

In this study, we investigated the spatio-temporal expression of pS80 MeCP2, pS421 MeCP2, and pS292 MeCP2 in the postnatal rat brain and preliminarily explored the function of MeCP2 in the developing cerebellum *via* shRNA-mediated MeCP2 deficiency.

Materials and Methods

Animals

Sprague-Dawley rats of embryonic day (E) 18, male rats of postnatal days (P) 1, 7, 14, 21, and 30, and adult rats used in this study were purchased from the Shanghai Experimental Animal Center, Chinese Academy of Sciences. All the animal protocols were approved by the Medical Experimental Animal Administrative Committee of Shanghai. All efforts were made to minimize animal suffering and reduce the number of animals used.

Western Blot Analysis

Preparation of Cytoplasmic and Nuclear Fractions

For the intracellular localization of MeCP2 and the pMeCP2s, we extracted cytoplasmic and nuclear proteins. P7, P14, and P30 rats were given an overdose of 10% chloral hydrate followed by removal of the brain, while E18 and P1 rats were sacrificed by rapid decapitation (n = 4–5 per group). Cytoplasmic and nuclear proteins were extracted from freshly-separated cortex and cerebellum at each age using a Nuclear and Cytoplasmic Protein Extraction Kit (Beyotime Institute of Biotechnology, Jiangsu, China) according to the manufacturer's instructions. Sixty milligrams of brain tissue was homogenized in 200 μL of a 20:1 mixture of reagents A and B with 1× protease inhibitor cocktail (PIC; Roche, Basel, Switzerland). After 15 min in an ice-bath, the lysate was centrifuged at 1,500×g for 5 min at 4 °C and the supernatant was collected as cytoplasmic proteins. Afterwards, the sediment of each 20 μL was re-suspended in 200 μL of reagent A containing 1× PIC followed by strong vortexing for 5 s. After incubation on ice for 10 min, 10 μL of reagent B was added to the suspension, and the mixture was vigorously vortexed and incubated in an ice-bath for

another 1 min. The supernatant was then removed following centrifugation at 12,000×g for 5 min. Afterwards, the precipitate from each 60 mg of tissue was fully re-suspended in 50 μL of reagent C with 1× PIC followed by ultrasonication. The supernatant fraction containing nuclear proteins was then collected by centrifugation at 16,000×g for 10 min at 4 °C. The protein concentration was quantified using a BCA protein assay kit according to the manufacturer's instructions (Beyotime Institute of Biotechnology). All samples were stored at −70 °C for further analysis.

Phosphatase Treatment

To validate the efficacy of the antibodies against the pMeCP2s, we treated cytoplasmic and nuclear extracts with alkaline phosphatase (PPTase; New England Biolabs, Ipswich, MA). The protein lysates were suspended in 1× NE buffer (New England Biolabs) at 20 μL buffer per microgram of protein. PPTase was added to the mixture, which was then incubated at 37 °C for 30 min. The proteins were then deposited in cold acetone at −20 °C overnight. After centrifugation at 16,000×g for 15 min, the purified proteins were obtained and re-suspended in 1× loading buffer for subsequent immunoblotting analysis. The controls received identical treatment but without PPTase.

Immunoblotting

To evaluate the expression levels of MeCP2 and the pMeCP2s, as well as those of neural cell markers nestin, doublecortin (DCX), neuron-specific class III β-tubulin (Tuj1), microtubule-associated protein 2 (MAP-2), calbindin-D28k (CB), and glial fibrillary acid protein (GFAP) in the developing rat brain, immunoblotting was performed as follows. Equal amounts of protein were separated on 8%–12% sodium dodecyl sulfate (SDS)-polyacrylamide gels and electrophoretically transferred to polyvinylidene difluoride membranes (Bio-Rad, Hercules, CA). The membranes were blocked with 10% (*w*/*v*) skim milk for 2 h, and then incubated with the following primary antibodies at 4 °C overnight: rabbit polyclonal antibody against MeCP2 (1:1000; Merck Millipore, Billerica, MA, Cat# 07-013, RRID: AB_2144004), pS80 MeCP2 (1:1000; Abgent, San Diego, CA, Cat# AP3595a, RRID: AB_2144008), pS421 MeCP2 (1:1000; Abgent, Cat# AP3693a, RRID: AB_10612715), pS292 MeCP2 (1:2000; US Biological, San Antonio, TX, Cat# M2763-30A, RRID: N/A), H3 (1:5000; Cell Signaling Technology, Danvers, MA, Cat# 9715, RRID: AB_331563); goat polyclonal antibody against DCX (1:2000; Santa Cruz Biotechnology, Dallas, TX, Cat# sc-8066, RRID: AB_2088), GFAP (1:2000; Abcam, HK, Cat# ab53554, RRID: AB_880202); mouse monoclonal antibody against nestin (1:1000; BD Pharmingen, Waltham, MA, Cat# 556309, RRID: AB_396354), Tuj1 (1:2000; Chemicon, Billerica, MA, Cat# MAB1637, RRID: AB_2210524), MAP-2 (1:2000; Sigma-Aldrich, St. Louis, MO, Cat# M9942, RRID: AB_477256), CB (1:5000; Sigma, Cat# C9848, RRID: AB_476894), GAPDH (1:5000; KangChen Bio-tech, Shanghai, China, Cat# KC-5G4, RRID: N/A), β-tubulin (1:5000; Sigma, T5293, RRID: AB_477580) or β-actin (1:10,000; Sigma, Cat# A5441, RRID: AB_476744). After washing, horseradish peroxidase-conjugated goat anti-rabbit IgG (1:3000; Santa Cruz), donkey anti-goat IgG (1:3,000; Santa Cruz) or goat anti-mouse IgG (1:3000; Santa Cruz) was incubated with the membranes at room temperature for 1 h. The blots were developed using enhanced chemiluminescence reagents (Santa Cruz) and Kodak X-OMAT film. The films were scanned and analyzed by measuring the optical density of immunostained bands in ImageJ (National Institutes of Health). Normalization was accomplished by stripping filters and re-probing for β-tubulin/β-actin for cytoplasmic proteins and H3 for nuclear proteins.

Histological Analysis

Tissue Preparation

Male rats at P7, P14 and P30 ($n = 3$–5 per group) were given an overdose of 10% chloral hydrate and transcardially perfused with 0.9% saline followed by 4% paraformaldehyde (PFA) in 0.1 mol/L phosphate-buffer solution (PBS; pH 7.4). Brains were removed and post-fixed in 4% PFA for 6 h and then sunk sequentially in 20% and 30% (*w*/*v*) sucrose in 0.1 mol/L PBS. Coronal or sagittal sections at 30 μm were then cut on a cryostat microtome (Leica CM3050s, Nussloch, Germany) and sections were stored at −20 °C in cryoprotectant for histological analysis. Sections were analyzed from at least two rats at each age.

Immunohistochemical Staining

To investigate the regional distribution of MeCP2 and the pMeCP2s and evaluate neural cell development (DCX, Tuj1, MAP-2, CB and GFAP), we performed immunohistochemical staining in the postnatal rat brain. Free-floating sections were incubated with 0.3% H_2O_2 at room temperature for 30 min and then with 0.01 mol/L trisodium citrate (pH 6.0) at 97.9 °C for 12 min. After rinsing in PBS for 15 min, the sections were blocked with 10% bovine serum in 0.01 mol/L PBS containing 0.3% Triton X-100 at 37 °C for 1 h and then incubated with the primary antibody

against MeCP2 (1:100), pS80 MeCP2 (1:50), pS421 MeCP2 (1:50), pS292 MeCP2 (1:100), GFAP (1:200), DCX (1:200), Tuj1 (1:200), MAP-2 (1:200), or CB (1:3,000) at 4 °C overnight. After washing, the sections were incubated with biotinylated anti-rabbit IgG (1:200; Vector Laboratories, Burlingame, CA), anti-goat IgG (1:200; Vector), or anti-mouse IgG (1:200; Vector) for 45 min at 37 °C followed by avidin-biotin-peroxidase (1:200; Vector) for 45 min at 37 °C. The immunoreactivity was visualized by 0.05% diaminobenzidine (Sigma) in Tris-HCl buffer (0.1 mol/L, pH 7.6) containing 0.03% H_2O_2. Negative controls received the same treatment except for the primary antibodies, and showed no specific staining. Images were acquired with a light microscope (Leica DMI6000B) in the somatosensory cortex, CA1 and dentate gyrus of the hippocampus and lobules 3–6 of the cerebellum. The brightness and contrast of the images were adjusted appropriately.

Immunofluorescence and Confocal Microscopy

To explore the cellular type distribution of MeCP2 and the pMeCP2s, we performed immunofluorescent triple-staining of MeCP2 or pMeCP2s with GFAP and NeuN/CB. Free-floating sections were first incubated with the primary antibody against MeCP2 (1:100), pS80 MeCP2 (1:50), pS421 MeCP2 (1:50), or pS292 MeCP2 (1:50) overnight at 4 °C and then with the secondary antibody rabbit anti-IgG-555 (1:500; Invitrogen, Waltham, MA) for 1 h at 37 °C. After rinsing in PBS, the sections were incubated with goat polyclonal anti-GFAP antibody (1:100) overnight at 4 °C followed by goat anti-IgG-488 (1:500; Invitrogen) at 37 °C for 1 h. After washing, the sections were incubated with mouse monoclonal anti-NeuN antibody (1:500; Millipore, Cat# MAB377, RRID: AB_229877) or mouse monoclonal anti-CB antibody (1:3000) overnight at 4 °C and then with mouse anti-IgG-Cy5 (1:200; Abcam) for 1 h at 37 °C. Finally, the sections were mounted on glass slides and coverslipped with fluorescence mounting medium (Vector).

To explore the intracellular localization of MeCP2 and the pMeCP2s, we performed fluorescent double-staining of MeCP2 or pMeCP2s with 4'6-diamidino-2-phenylindole dihydrochloride (DAPI). The sections were first incubated with the primary antibody against MeCP2, pS80 MeCP2, pS421 MeCP2, or pS292 MeCP2 and then with the secondary antibody rabbit anti-IgG-555 as described above. After washing in PBS, the sections were further stained with DAPI (1 μg/mL; Invitrogen) for 10 min at room temperature. Finally, the sections were washed, mounted, and coverslipped.

The fluorescent signals were detected at an excitation wavelength of 555 nm and emission wavelengths of 565 nm (IgG-555), 488 nm and 525 nm (IgG-488 and FITC), 650 nm and 667 nm (Cy5), and 358 nm and 461 nm (DAPI) by confocal laser scanning microscopy (Leica TCS SP5). Images were acquired using Leica software (Leica TCS SPE) at a thickness of 6–8 μm (1024 × 1024 pixel resolution) in the somatosensory cortex and cerebellar lobules 3–6. The brightness and contrast of the images were adjusted appropriately.

RNA Isolation and Quantitative RT-PCR (RT-qPCR) Analysis

To evaluate the time-course of neural cell development, the mRNA levels of *Dcx*, *Tuj1*, *Map-2*, and *Gfap* were assessed in the postnatal rat brain. Total RNA was extracted from the rat cerebellum at P7, P14, and P30 ($n = 6$ per group) using TRIzol (Invitrogen) according to the manufacturer's instructions. In brief, 100 mg cerebellum was homogenized in 1 mL TRIzol. After incubation at room temperature for 5 min, 200 μL chloroform per milliliter TRIzol was added. The mixture was blended by shaking the tube vigorously for 15 s followed by incubation for another 5 min at room temperature. After centrifugation at 12,000×g for 15 min, the upper aqueous phase was removed to a new tube containing 500 μL isopropanol then allowed to precipitate for 1 h at −20 °C. The RNA pellets were collected following centrifugation at 12,000×g for 10 min, and then washed twice with 75% ethanol. After air-drying for 5 min, the RNA precipitate was re-suspended in 20 μL diethyl pyrocarbonate-treated sterile water. Total RNA (5 μg) from each sample was reverse-transcribed into cDNA in the presence of 1 μL M-MuLV reverse transcriptase (200 U/μL; Invitrogen), 2 μL of 10 mmol/L dNTPs (TaKaRa, Shiga, Japan), and 1 μL oligo (dT). Quantitative PCR analysis was performed with Mastercycler Realplex (Eppendorf, Hamburg, Germany) using SYBR Green Realtime PCR Master Mix (Toyobo, Osaka, Japan). The primers were: *Tuj1* forward, tagaccccagcggcaactat; *Tuj1* reverse, gttccaggttccaagtccacc (PrimerBank); *Dcx* forward, ggggattgtgtacgctgttt; *Dcx* reverse, cgaccagttgggattgacat; *Map-2* forward, caaacgtcattactttacaacttg; *Map-2* reverse, cagctgcctctgtgagtgag; *Gfap* forward, ggtggagagggacaatctc; *Gfap* reverse, ccagctgctcctggagttct [26]; *β-actin* forward, gtcttcccctccatcgtggg; *β-actin* reverse, tggctggggtgttga aggtc.

MeCP2 shRNA Interference

Plasmid Injection

To explore the function of MeCP2 in the postnatal cerebellum, its endogenous expression was inhibited *via* shRNA injection. cDNA plasmids encoding small-hairpin

RNA (shRNA) interfering sequences were from Santa Cruz Biotechnology. These plasmids were a mixture of target-specific vector plasmids encoding several 19–25 nt (plus hairpin) shRNAs designed to knock down *Mecp2* expression (Santa Cruz). Another shRNA plasmid encoding a scrambled sequence that would not lead to the specific degradation of any known cellular mRNA sequence was used as a control for shRNA off-target effects (Santa Cruz). Rats at P7 were randomly divided into an MeCP2 shRNA group and a control shRNA group. A mixture containing 1 μg plasmids in 9 μL of 0.9% (*w*/*v*) sterile sodium chloride solution and 1 μL of Lipofectamine 2000 (Invitrogen) was injected into the cisterna magna as previously described [27]. Briefly, a 26-G needle of a 1-mL syringe was bent to a 45° angle 4 mm from the tip. An injection was made by inserting the tip of the needle into the foramen magnum between the occipital bone and the first cervical vertebra. After injection, rat pups were returned to their dams until they were weaned. Protein extracts ($n = 4$ or 8 per group) and tissue samples ($n = 3$ per group) were then prepared from the cerebellum at P14 and P30.

Whole-Cell Protein Extraction

Western blot analysis was performed to determine the effects of MeCP2 knockdown on the expression of neural cell marker proteins. Rat cerebellum treated with control or MeCP2 shRNA was dissected and homogenized in RIPA buffer (1× PBS, 1% Nonidet P-40, 0.5% sodium deoxycholate, 0.1% SDS, and 1 mmol/L sodium orthovanadate)

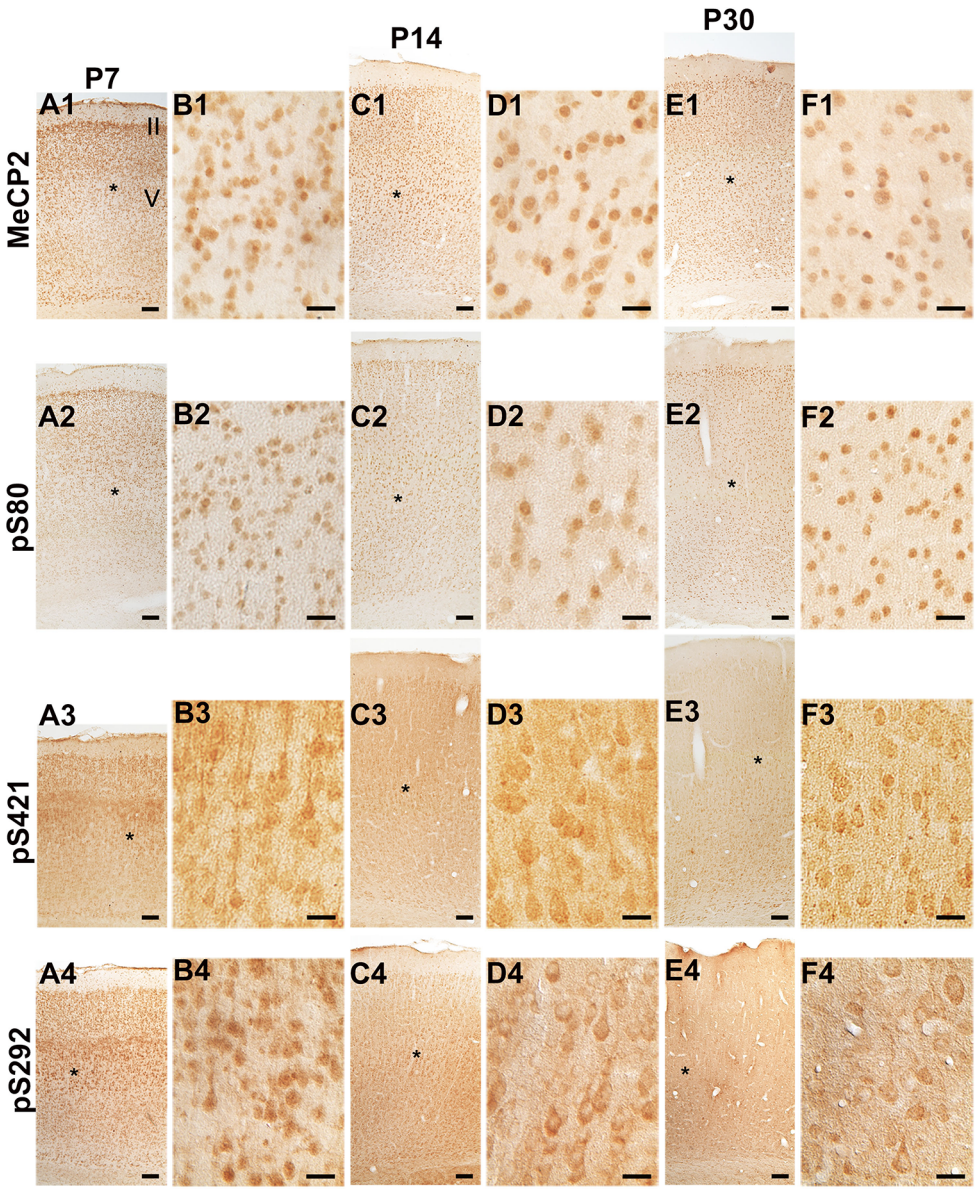

Fig. 1 Regional distribution of MeCP2 and diverse phospho-MeCP2s (pMeCP2s) in postnatal rat cortex. MeCP2 (**A1**–**F1**) and pS80 MeCP2 (**A2**–**F2**) exhibited a nuclear distribution and became distributed more uniformly with maturation of the brain. pS421 MeCP2 (**A3**–**F3**) and pS292 MeCP2 (**A4**–**F4**) staining was mainly in the cytoplasm and neurites, and this was markedly attenuated at P30. **B**, **D**, and **F** are magnifications of the *asterisk*-marked areas in **A**, **C**, and **E**. *Scale bars* 100 μm in **A**, **C**, and **E**; 20 μm in **B**, **D**, and **F**. The negative control without the primary antibody is shown in Fig. S3.

containing 1× PIC. After 30 min in an ice-bath, the lysate was centrifuged at 12,000×g for 30 min at 4 °C and the supernatant was collected as the whole-cell proteins. The protein concentration was quantified as above. All samples were stored at −70 °C for further western blot analysis.

Statistical Analysis

SPSS 13.0 (IBM, Chicago, IL) was used for statistical analysis. Data are presented as the mean ± SEM. One-way ANOVA was used for multiple-group comparisons, and unpaired Student's *t*-test for two-group comparisons. $P < 0.05$ was considered statistically significant.

Results

Regional Distribution of MeCP2 and Diverse pMeCP2s in the Postnatal Rat Brain

Layer V cells in the cortex of P7 rats were darkly stained for MeCP2, and layer II had the highest density of positive cells (Fig. 1A1, B1). At P14, the MeCP2-labeled cells were more uniformly distributed in layers II–V (Fig. 1C1, D1). At P30, the density of MeCP2-positive cells was similar to that at P14 although the staining was less intense (Fig. 1E1, F1). The distribution pattern of pS80 MeCP2 (Fig. 1A2–F2) resembled that of MeCP2. The distribution of pS421

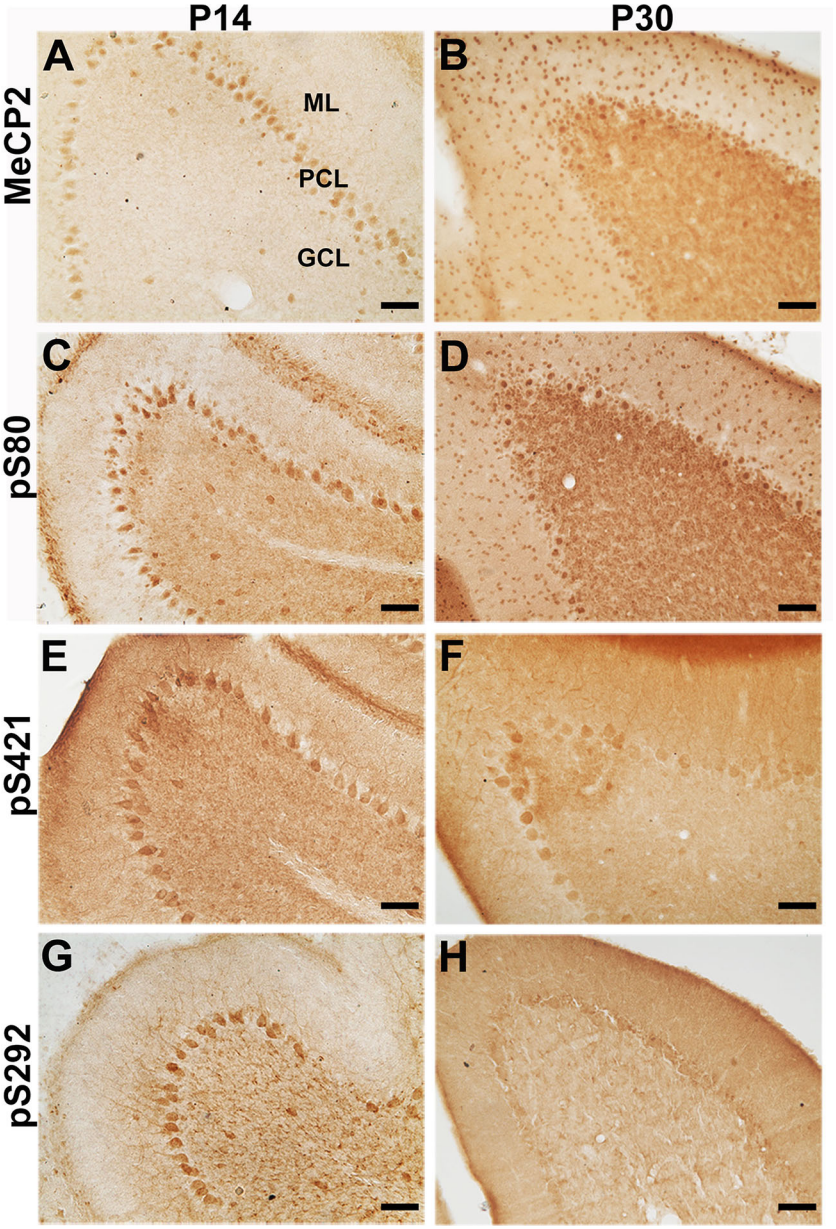

Fig. 2 Regional distribution of MeCP2 and diverse pMeCP2s in the postnatal rat cerebellum. MeCP2 and the pMeCP2s were apparently expressed in the PCL at both P14 and P30. MeCP2 (**A**, **B**) and pS80 MeCP2 (**C**, **D**) were mostly localized in the nuclei and became more widely distributed with maturation. pS421 MeCP2 (**E**, **F**) and pS292 MeCP2 (**G**, **H**) were mainly localized in the cell bodies and neurites and were markedly reduced by P30. *Scale bars* 50 μm. *ML* molecular layer, *PCL* Purkinje cell layer, *GCL* granule cell layer. The negative control without the primary antibody is shown in Fig. S3.

MeCP2 was similar to that of MeCP2 at P7 (Fig. 1A3, B3), while the intensity and density of pS421 MeCP2 immunoreactivity at P14 was more homogeneous in the different layers despite the presence of more darkly-stained cells in layer V (Fig. 1C3, D3). In contrast, the density and intensity of pS421 MeCP2 immunoreactivity in the cortical layers were markedly decreased at P30 (Fig. 1E3, F3). pS292 MeCP2 showed a distribution pattern similar to that of pS421 MeCP2 (Fig. 1A4–F4).

In the cerebellum, the distribution patterns of MeCP2 and the pMeCP2s were cell-specific (Fig. 2). At P14, they were primarily expressed in the Purkinje cell layer (PCL) with some staining in the granule cell layer (GCL) (Fig. 2A, C, E, G). At P30, much of the MeCP2 and pS80 MeCP2 staining appeared in the molecular layer (ML), while their immunoreactivity in the PCL was similar to that at P14. Moreover, the immunoreactivity of MeCP2 and pS80 MeCP2 in the GCL were also greatly intensified despite the lack of a clear cellular distribution (Fig. 2B, D), consistent with a previous study [10]. However, the immunoreactivity of pS421 MeCP2 and pS292 MeCP2 became much weaker in the P30 PCL than that at P14. The pS421 and pS292 MeCP2-positive cells were still absent from the ML, with some weak staining in the GCL (Fig. 2F, H).

MeCP2 and the pMeCP2s were densely expressed throughout the hippocampus (Fig. 3). At P7, their immunoreactivity was stronger in the pyramidal cell layer of CA1 than in the GCL of the dentate gyrus (DG) (Fig. 3A–C). With development, the immunoreactivity of MeCP2 at P14 remained similar to that at P7 in CA1, but that of pMeCP2s was weaker. However, their staining in the DG was intensified (Fig. 3D–F). In the P30 hippocampus, MeCP2- and pS80 MeCP2-positive cells were more clearly distributed in both CA1 and the DG, but the intensity did not differ from that at P14. In contrast, the immunoreactivity of pS421 MeCP2 and pS292 MeCP2 declined throughout the hippocampus at P30 (Fig. 3G–I). Taken together, these findings revealed development-associated changes in the regional distribution of MeCP2 and the pMeCP2s in the postnatal rat brain.

Expression Patterns of MeCP2 and Diverse pMeCP2s in the Developing Rat Brain

First, we tested the specificity of the antibodies against the diverse pMeCP2s. When the phosphate groups of the proteins were eliminated by adding PPTase to the protein lysates, the bands for pS80 MeCP2 (60 kD), pS421 MeCP2 (58 kD), and pS292 MeCP2 (77 kD) were abolished (Fig. 4A),

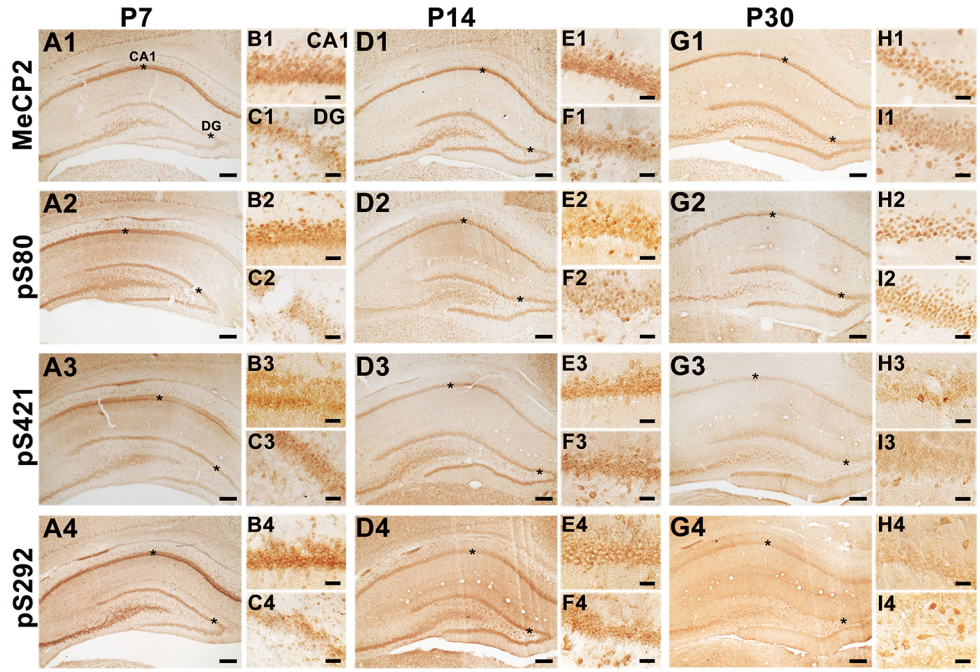

Fig. 3 Regional distribution of MeCP2 and diverse pMeCP2s in the postnatal rat hippocampus. MeCP2 (**A1**–**I1**), pS80 MeCP2 (**A2**–**I2**), pS421 MeCP2 (**A3**–**I3**), and pS292 MeCP2 (**A4**–**I4**) were expressed throughout the hippocampus from P7 to P30. MeCP2- and pS80 MeCP2-positive cells became more evident with maturation, while the immunoreactivity of pS421 MeCP2 and pS292 MeCP2 was weaker at P30. **B** and **C**, **E** and **F**, and **H** and **I** are magnifications of the *asterisk*-marked areas in **A**, **D**, and **G**. **B**, **E**, and **H** are from **CA1**, and **C**, **F**, and **I** are from the DG. *Scale bars* 150 μm in **A**, **D**, and **G**; 25 μm in **B** and **C**, **E** and **F**, and **H** and **I**. *DG* dentate gyrus. The negative control without primary antibody is shown in Fig. S3.

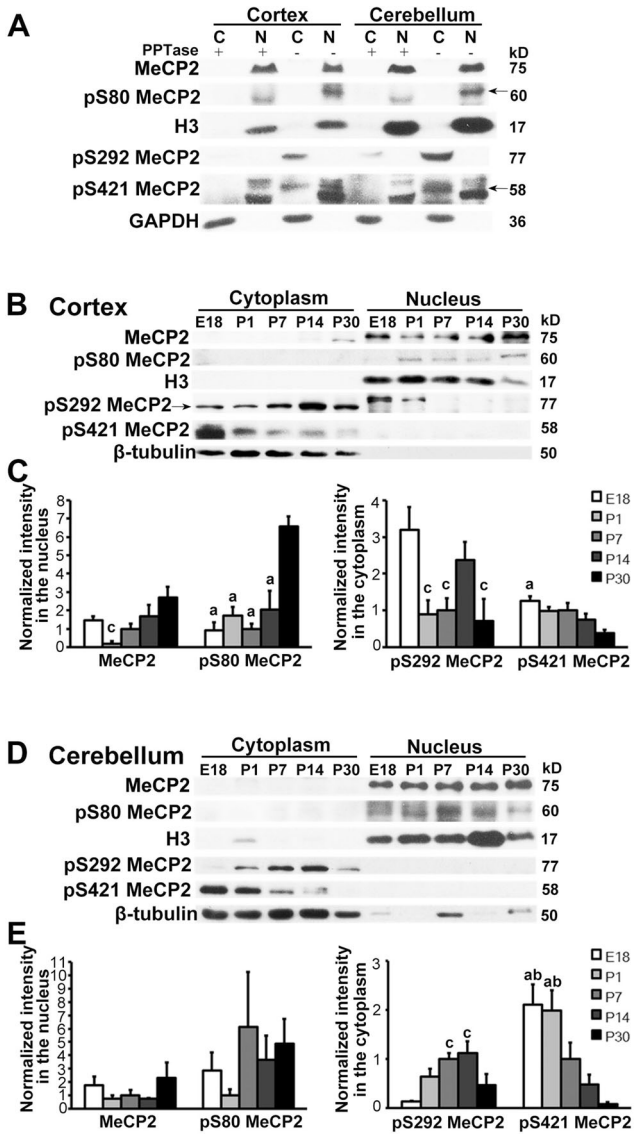

Fig. 4 Distinct expression and intracellular localization of MeCP2 and the pMeCP2s in the developing rat brain. Western blot analysis was applied to the cytoplasmic and nuclear proteins. The specificity of antibodies against pS80 MeCP2 (~60 kD), pS421 MeCP2 (~58 kD), and pS292 MeCP2 (~77 kD) was validated by the application of PPTase to the protein extracts from cortex and cerebellum at P14 (**A**). MeCP2 (75 kD) and pS80 MeCP2 were mainly found in the nuclear fraction, while pS292 MeCP2 and pS421 MeCP2 were mainly in the cytoplasm. The temporal patterns of expression of MeCP2 and the pMeCP2s were distinct in the cortex (**B**, **C**) and cerebellum (**D**, **E**). *Arrows* show the positions of pS80 MeCP2, pS421 MeCP2, and pS292 MeCP2. GAPDH and β-tubulin were used as loading controls for the cytoplasmic proteins, and H3 for the nuclear proteins. The data are normalized to the values at P7 (mean ± SEM; $n = 4$–5 per group; $^{a}P < 0.05$ *vs* P30, $^{b}P < 0.05$ *vs* P14, $^{c}P < 0.05$ *vs* E18). *C* cytoplasm, *N* nucleus, *PPTase* phosphatase. Blots over the range from 50 to 80 kD are shown in Fig. S4.

demonstrating the efficacy of the antibodies in recognizing the pMeCP2s. Furthermore, MeCP2 (75 kD) and pS80 MeCP2 were predominant in the nuclear fraction, while pS421 MeCP2 and pS292 MeCP2 were expressed in the cytoplasm (Fig. 4A, B, D). On this basis, we assessed their expression levels in the developing rat brain. In the cortex (Fig. 4B, C), MeCP2 and pS292 MeCP2 were expressed at a relatively high level at E18, decreased by P1 ($P = 0.001$ for MeCP2 and $P = 0.021$ for pS292), and then gradually rose from P1 to P14. At P30, the expression of MeCP2 was further increased, whereas that of pS292 MeCP2 was decreased. The expression of pS421 MeCP2 was maintained at a high level from E18 to P14, then was reduced at P30 ($P = 0.031$ *versus* P7). Conversely, pS80 MeCP2 was expressed at a relatively low level from E18 to P14, and was increased at P30 ($P = 0.005$ *versus* P14). In the cerebellum (Fig. 4D, E), the expression patterns of MeCP2 and the pMeCP2s were similar to those in the cortex, except that the level of pS292 MeCP2 at E18 was much lower than those postnatally, and MeCP2 expression did not increase until P30, together with an earlier decline for pS421 MeCP2 (P7) and an earlier rise for pS80 MeCP2 (P14). Taken together, these results demonstrated that the expression patterns of MeCP2 and the pMeCP2s are distinct in the developing rat brain.

Intracellular Localization of MeCP2 and Diverse pMeCP2s in the Postnatal Rat Brain

To confirm the intracellular localization of MeCP2 and the pMeCP2s, we performed immunofluorescent double-staining with DAPI in the rat cortex and found that MeCP2 (Fig. 5A, B) and pS80 MeCP2 (Fig. 5C, D) were completely co-localized with DAPI, while pS421 MeCP2 (Fig. 5E, F) and pS292 MeCP2 (Fig. 5G, H) were mostly excluded and surrounded the nucleus at both P14 and P30, consistent with the findings of western blot analysis (Fig. 4). These results demonstrated that the intracellular localizations of MeCP2 and the pMeCP2s are distinct in the postnatal rat brain.

Cell Types Expressing MeCP2 and the pMeCP2s in the Postnatal Rat Brain

In the cortex, MeCP2 and the pMeCP2s were all primarily expressed in neurons ($NeuN^{+}$) at P14 and P30 (Fig. 6). Moreover, MeCP2 was observed in a few astrocytes (Fig. 6A, B), consistent with previous findings [11, 28]. Interestingly, pS80 MeCP2, pS421 MeCP2, and pS292 MeCP2 were also detected in astrocytes, although double-labeled cells were extremely few (Fig. 6C–H). In the cerebellum, immunofluorescent triple-staining of MeCP2 and the pMeCP2s with GFAP and CB, a marker for Purkinje cells, showed that MeCP2 and the pMeCP2s were predominantly expressed in Purkinje cells at both P14 and P30 (Fig. 7). Moreover, their signals also appeared in the

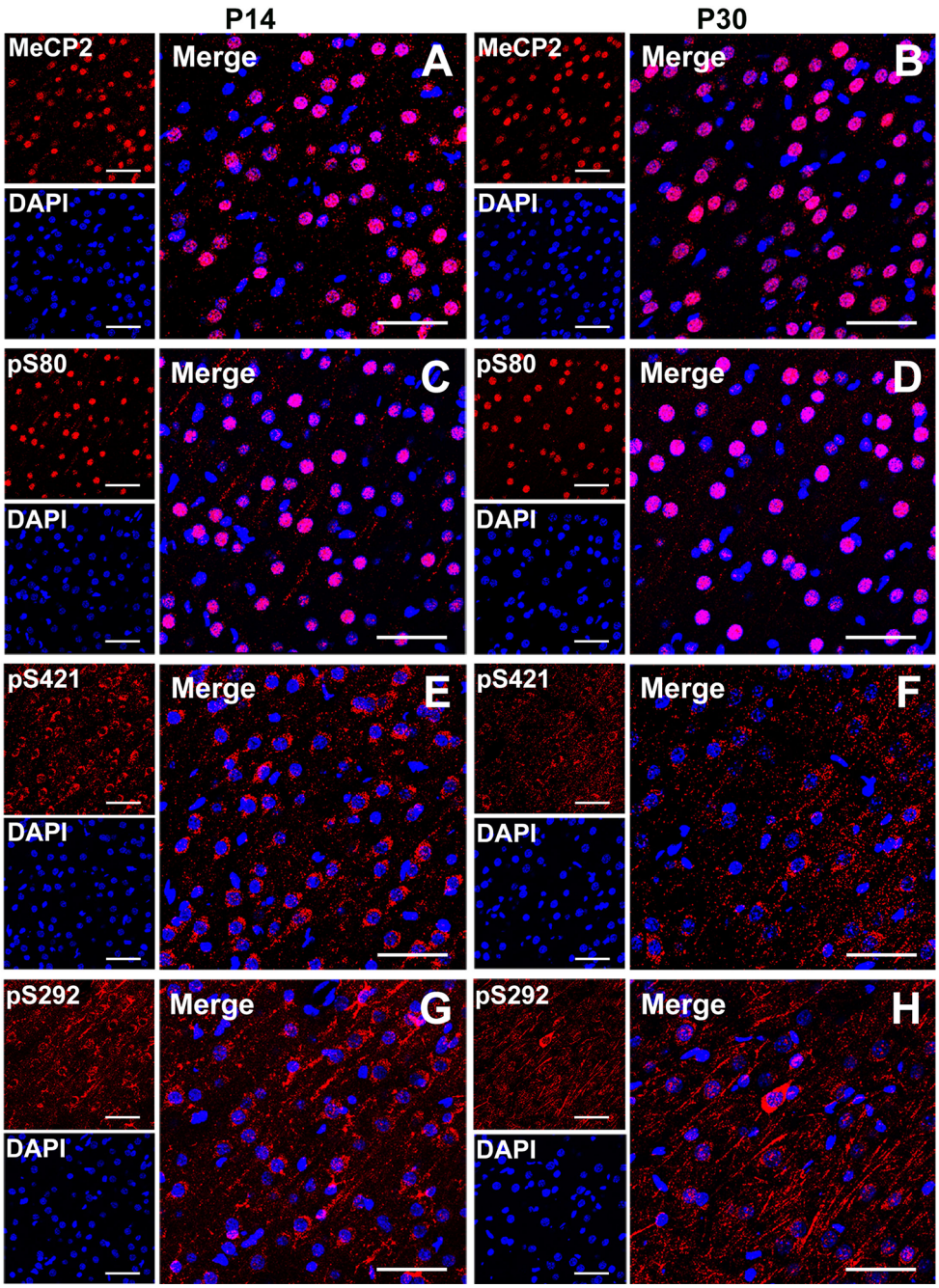

Fig. 5 Intracellular localization of MeCP2 and the pMeCP2s in the postnatal rat cortex. Confocal images of immunofluorescent double-staining of MeCP2, pS80 MeCP2, pS421 MeCP2, or pS292 MeCP2 (*red*) with DAPI (*blue*) in the rat cortex at P14 and P30. MeCP2 (**A**, **B**) and pS80 MeCP2 (**C**, **D**) were co-localized with DAPI, whereas pS421 MeCP2 (**E**, **F**) and pS292 MeCP2 (**G**, **H**) were mostly excluded from and enwrapped the DAPI-labeled nucleus. *Scale bars* 50 μm.

GCL at P14 (Fig. 7A1–A4) and in the ML at P30 (Fig. 7C1–C4), generally consistent with the immunohistochemical results (Fig. 2) and previous findings [10]. Importantly, MeCP2 and the pMeCP2s were also co-labeled with GFAP in the GCL, although the number was small (Fig. 7B1–B4, D1–D4). Taken together, these results demonstrated that MeCP2 and the pMeCP2s are mainly expressed in neurons in the postnatal rat brain.

Function of MeCP2 in Neural Cell Development in the Postnatal Rat Cerebellum

First, we assessed the mRNA and protein levels of development-associated neuronal and astrocytic markers in the postnatal rat cerebellum. The results showed that the expression of a stem cell marker (nestin) and immature cell markers (DCX and Tuj1) declined with

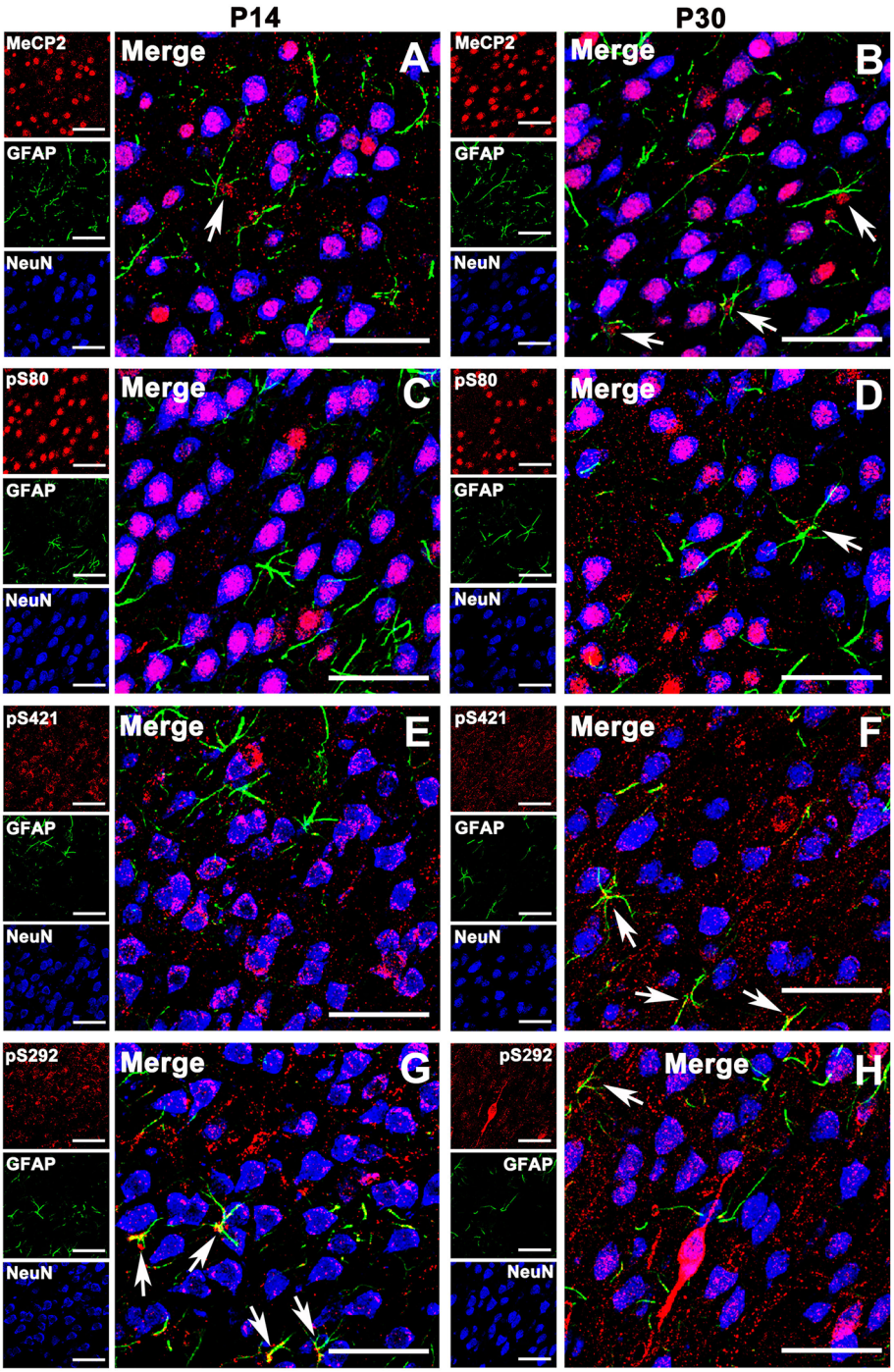

Fig. 6 Cellular types expressing MeCP2 and the pMeCP2s in the postnatal rat cortex. Confocal images of immunofluorescent triple-staining of MeCP2 (**A**, **B**), pS80 MeCP2 (**C**, **D**), pS421 MeCP2 (**E**, **F**), or pS292 MeCP2 (**G**, **H**) (*red*) with GFAP (*green*) and NeuN (*blue*) at P14 and P30. MeCP2 and the pMeCP2s were mainly expressed in neurons. They were also expressed in astrocytes at a low level (*arrows*). *Scale bars* 50 μm.

development, while the mature cell markers (MAP-2, CB, and GFAP) increased (Fig. S1). Then, we delivered MeCP2 shRNA-expressing plasmids into the cisterna magna of P7 rats and assessed the levels of neural cell markers by western blot and immunohistochemistry in the cerebellum at P14 and P30 (Fig. 8A). The data showed that the expression of MeCP2 was lower in the MeCP2 shRNA group than in the control shRNA group at both P14 ($P = 0.001$, Fig. 8B, C) and P30 ($P = 0.07$, Fig. 8D, E), indicating successful suppression of endogenous MeCP2 expression. At P14, the neuron-specific markers DCX, Tuj1, MAP2, and CB were not affected by MeCP2 deficiency, but the astrocytic marker GFAP was reduced ($P = 0.01$) (Fig. 8B, C). At P30, the expression of GFAP was not changed, while DCX, Tuj1, and CB were decreased and MAP-2 was increased after MeCP2 knockdown ($P = 0.07$ for DCX, $P = 0.06$ for Tuj1, $P = 0.001$ for CB, and $P = 0.01$ for MAP-2). To confirm

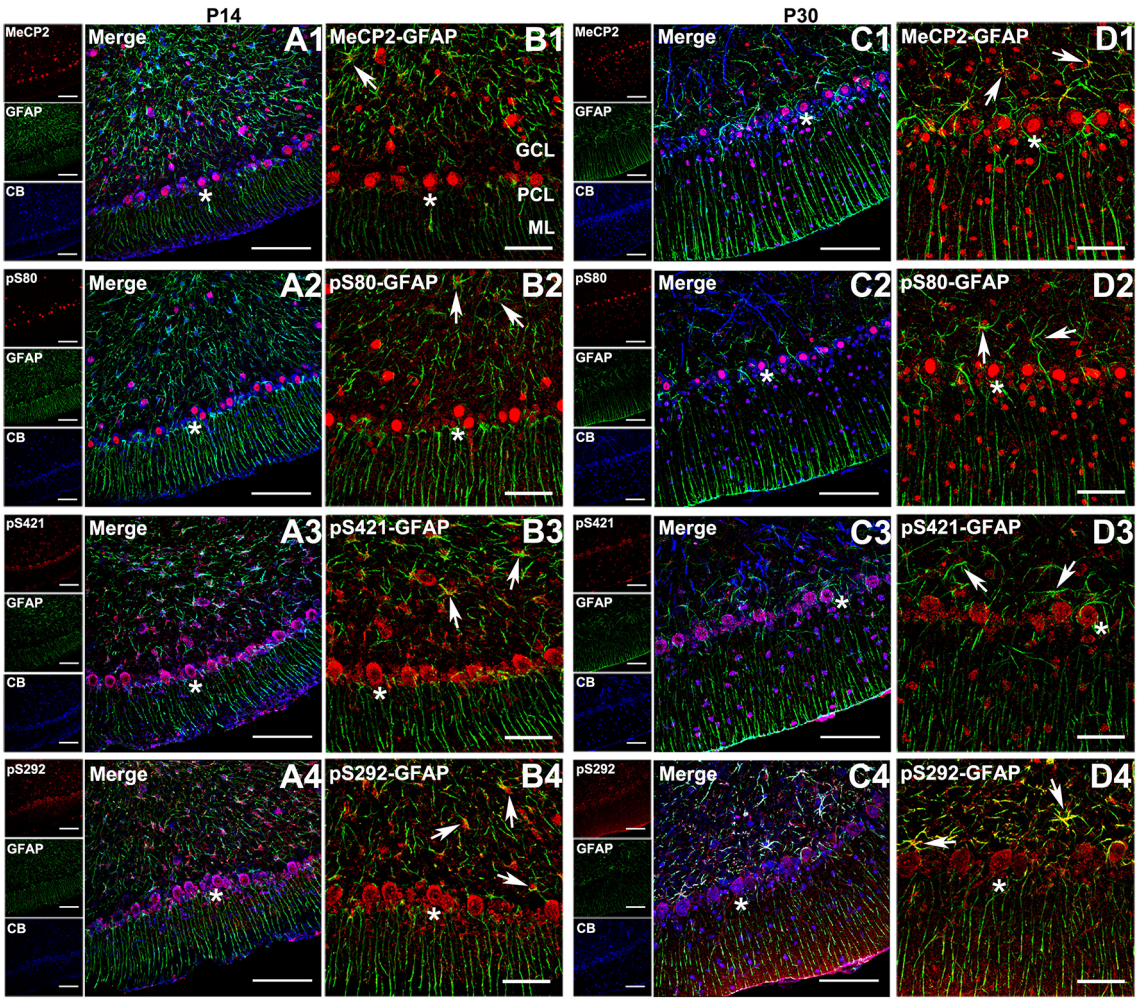

Fig. 7 Cell types expressing MeCP2 and the pMeCP2s in the postnatal rat cerebellum. Confocal images of immunofluorescent triple-staining of MeCP2 (**A1–D1**), pS80 MeCP2 (**A2–D2**), pS421 MeCP2 (**A3–D3**), or pS292 MeCP2 (**A4–D4**) (*red*) with GFAP (*green*) and CB (*blue*), a marker for Purkinje cells, at P14 and P30. MeCP2 and the pMeCP2s were predominantly expressed in Purkinje cells (**A**, **C**). They were also co-localized with GFAP in the GCL at a low level (**B**, **D**, *arrows*). **B** and **D** are the magnifications of the *asterisk*-marked areas in **A** and **C**. *Scale bars* 100 μm in **A** and **C**; 50 μm in **B** and **D**. A magenta-green version of the images in **B** and **D** is shown in Fig. S2.

these results, we further performed immunohistochemical single-staining of DCX, Tuj1, MAP-2, CB, or GFAP (Fig. 8F–O). At P14, the GFAP signal appeared much weaker after MeCP2 shRNA knockdown (Fig. 8F, G). In the P30 cerebellum, the immunoreactivity of DCX (Fig. 8H, I) and Tuj1 (Fig. 8J, K) was lower in the MeCP2 shRNA group than in the control shRNA group. In contrast, the immunoreactivity of MAP-2 was greatly increased after MeCP2 knockdown, together with increased complexity of neuronal branches in the ML (Fig. 8L, M). Meanwhile, the Purkinje cells were more lightly stained by CB in the MeCP2-deficient group (Fig. 8N, O). Taken together, these results demonstrated that MeCP2 deficiency initiated postnatally disturbs neural cell development in the rat cerebellum.

Discussion

In this study, we examined the expression and distribution of MeCP2, pS80 MeCP2, pS421 MeCP2, and pS292 MeCP2 in the postnatal rat brain. We found that the patterns of expression and distribution of MeCP2 and the diverse pMeCP2s were distinct and varied with brain development. MeCP2 and pS80 MeCP2 were concentrated in the nucleus, whereas pS421 MeCP2 and pS292 MeCP2 were mainly localized in the cytoplasm. Moreover, MeCP2 and the pMeCP2s were predominantly expressed in neurons, but they were also expressed in astrocytes at a relatively low level. Importantly, postnatal MeCP2 deficiency in the rat cerebellum disturbed the subsequent neural cell development. These results demonstrated that MeCP2 and

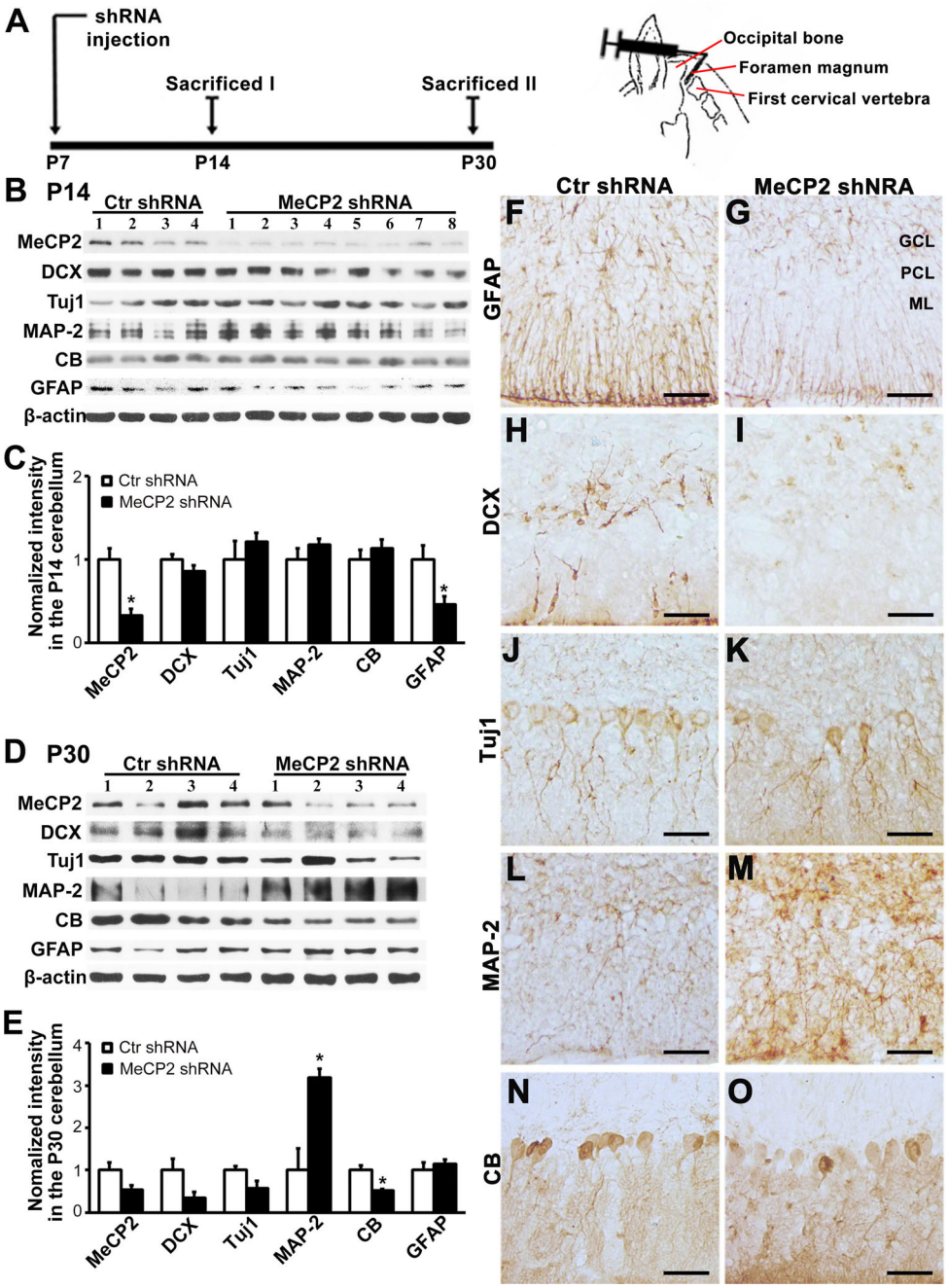

Fig. 8 Function of MeCP2 in neural cell development in the postnatal rat cerebellum. **A** Cartoon showing the injection of MeCP2 shRNA into the cisterna magna at P7. **B**–**E** Western blot analysis showing that the expression of endogenous MeCP2 was inhibited at P14 (**B**, **C**) and P30 (**D**, **E**). At P14, the protein levels of DCX, Tuj1, MAP-2, and CB were not changed, whereas that of GFAP was reduced by MeCP2 knockdown. At P30, DCX and Tuj1 were decreased, while MAP-2 was increased by MeCP2 shRNA. The expression of CB was also reduced, but that of GFAP was not altered. **C** and **E** show the statistical results of **B** and **D**. **F**–**O** Immunohistochemical images of GFAP (**F**, **G**) at P14, and of DCX (**H**, **I**), Tuj1 (**J**, **K**), MAP-2 (**L**, **M**), and CB (**N**, **O**) at P30 showed similar results. β-actin was used as a loading control for western blot analysis. The data are normalized by the values in the control group (mean ± SEM; $n = 4$ or 8 per group; $^*P < 0.05$ *vs* control shRNA group; *scale bars* 50 μm). *Ctr* control.

the pMeCP2s have distinct temporal expression and spatial distribution, and that the precise level of MeCP2 in the postnatal period is vital for neural cell development in the rat cerebellum.

Expression of Diverse pMeCP2s

The expression and distribution of MeCP2 in the brain has been thoroughly studied. It is detectable in rodent cortex and cerebellum from E14. With development, its expression gradually rises and achieves its highest level in the adult brain. In cortex, its expression spreads from the inner to the outer layers and its distribution becomes more uniform as the rat brain matures. In the cerebellum, MeCP2 staining is limited to Purkinje cells and Golgi cells, the cell types generated earliest in the first three postnatal weeks, and then emerges in stellate cells and granule cells [10, 29]. Consistently, in this study, we also found that the expression of MeCP2 increased with brain maturation (Fig. 4), and that its regional distribution (Figs. 1, 2, 3) was similar to that in a previous study [10].

To date, the patterns of expression of pMeCP2s remain unclear. Here, we examined the expression and distribution of pS80 MeCP2, pS421 MeCP2, and pS292 MeCP2 in the postnatal brain and found that pS80 MeCP2 was significantly increased in the mature brain. Moreover, the distribution of pS80 MeCP2 in the postnatal cortex, cerebellum, and hippocampus was similar to that of MeCP2. Conversely, pS421 and pS292 MeCP2 were lower in the mature brain than their relatively high levels of expression in the early postnatal period (Figs. 1, 2, 3, 4). Given that pS421 MeCP2 is triggered by membrane depolarization while pS80 MeCP2 is established under resting conditions in neurons [3, 4], together with their predominant expression in neurons, their contrary expression during brain development is not unexpected. Notably, pS292 MeCP2, a new form of pMeCP2, seems quite special. The increase of pS292 MeCP2 from P1 to P14 was similar to that of MeCP2, but its decrease at P30 resembled that of pS421 MeCP2 (Figs. 1, 2, 3, 4). In a recent study, we showed that pS292 MeCP2 expression is induced in the ischemia-injured adult rat brain, raising the possibility that pS292 MeCP2 responds rapidly to environmental change [8]. These results suggest that MeCP2 has multiple functions in the modulation of brain development during different postnatal periods *via* its dynamic phosphorylation at different serine sites.

Intracellular Localization of Diverse pMeCP2s

So far, most researchers have considered MeCP2, pS80 MeCP2, and pS421 MeCP2 to be nucleoproteins [6, 9, 30]. Nevertheless, one study has shown that MeCP2 is detectable in the cytoplasm of undifferentiated PC12 cells in a phosphorylated form [13]. Consistent with this, we have also shown that pS292 MeCP2 is predominantly distributed in the cytoplasm of neural cells in the adult rat striatum, in contrast with the nuclear localization of MeCP2 [8]. In the present study, we found that MeCP2 and pS80 MeCP2 were mainly concentrated in the nucleus (Figs. 4, 5), in accord with previous reports [9, 30]. On the contrary, pS421 MeCP2 and pS292 MeCP2 were primarily detected in the cytoplasm (Figs. 4, 5). Together with the expression levels of diverse pMeCP2s in the postnatal brain (Fig. 4), our data imply that MeCP2 is translocated from the cytoplasm to the nucleus *via* phosphorylation at diverse serine sites as the brain matures. Studies on the dynamic cytoplasmic-nuclear transport of MeCP2 are still needed to directly demonstrate this intracellular relocation. As pS421 MeCP2 can be isolated from the target genes in depolarized neurons [3], it is possible that released pS421 MeCP2 is relocated from nucleus to cytoplasm to terminate its action as a transcriptional modulator and/or to play an additional role in cytoplasmic processes. Notably, pS292 MeCP2 had a cytoplasmic distribution similar to pS421 MeCP2. These findings imply that pS421 MeCP2 and pS292 MeCP2 share common functions, phosphorylation pathways, and/or transport mechanisms in the brain.

Phenotype of Cells Expressing Diverse pMeCP2s

It is well documented that MeCP2, pS80 MeCP2, and pS421 MeCP2 are primarily expressed in neurons [4, 5, 31], and that neuronal MeCP2 is vital for maintaining normal brain development [32–34]. Recently, studies have further shown that MeCP2 is also detectable in glial cells at significantly lower levels. Astrocyte-derived MeCP2 is critical for the normal development of astrocytes and neurons [11, 35, 36]. Consistently, we found here that MeCP2, pS80 MeCP2, pS421 MeCP2, and pS292 MeCP2 were all predominantly expressed in neurons at P14 and P30 in the rat (Figs. 6, 7). Moreover, MeCP2 and pS292 MeCP2 were also detected in a few astrocytes, in general agreement with previous studies [8, 11, 36]. Conversely, we found pS80 MeCP2 and pS421 MeCP2 expression in astrocytes, in contrast to the previous findings of neuronal localization [4, 5]. Interestingly, Maezawa *et al.* [36] have shown that MeCP2 deficiency progressively spreads between MeCP2-deficient and wild-type astrocytes *via* gap junctions. Considering the cytoplasmic and astrocytic distribution of pS421 MeCP2 and pS292 MeCP2, they may be messengers between astrocytes involved in the spread of MeCP2 deficiency.

Function of MeCP2 in the Postnatal Rat Cerebellum

The role of MeCP2 in neural cell development is still controversial. Tsujimura *et al.* [37] have reported that MeCP2 overexpression actually regulates the differentiation of neural precursor cells by suppressing astrogenesis and promoting neurogenesis. In contrast, Kishi and Macklis [38] showed that MeCP2 is involved in neuronal maturation rather than cell-fate decisions using an *Mecp2* mutant neural precursor cell model. These results suggest that the function of MeCP2 in brain development is complex and needs further investigation. In this study, we found that nestin, a marker for neural stem cells, was expressed at E18 and P1 but was reduced to an extremely low level thereafter (Fig. S1), indicating that differentiation-related events are slowed or even arrested after P7 in the rat cerebellum. On the other hand, the markers for mature neurons, such as MAP-2 and CB, exhibited a gradual increase after P7, and the markers for immature neurons, such as DCX and Tuj1, were significantly decreased by P30. These findings indicate that maturation-associated events become dominant from P7 and P30. Together with the enhanced expression of MeCP2 with brain development (Fig. 4), these data

imply that MeCP2 plays a more important role in the mature brain.

Generally, RTT patients are characterized by germline mutations in *MECP2*. On this basis, previous studies were mostly conducted on mouse models with *Mecp2* mutations initiated from the germline [21, 22, 39]. However, the finding that the symptoms of RTT can be reversed in adult mice upon global restoration of MeCP2 suggests a potential role for MeCP2 in adulthood [23]. Recent studies have further shown that the inducible loss of MeCP2 after birth also causes RTT-like phenotypes. MeCP2-deficiency in the postnatal and adult mouse not only elicits brain shrinkage with a higher density of neurons, but also results in retracted neuronal dendritic arbors and reduced complexity of astrocytic processes. These findings indicate that MeCP2 is required for the late stages of brain maturation [24, 40, 41]. To date, however, few investigations have focused on the postnatal function of MeCP2 in the cerebellum, dysfunction of which may be correlated with the motor deficits in RTT patients. Here, we found that MeCP2 expression at P14 was significantly reduced by MeCP2 shRNA, indicating the successful knockdown of MeCP2 expression in the cerebellum. Notably, despite applying different interference methods (Fig. 8A), our animal models showed a degree of decrease in MeCP2 expression at one week after shRNA treatment (32.5% of its normal level) similar to that previously described [24]. Moreover, we found a remarkable decrease of GFAP expression, but no significant changes in DCX, Tuj1, MAP-2, or CB expression, in the MeCP2 shRNA group (Fig. 8B, C, F, G). At P30, although the MeCP2 expression was still knocked down by the shRNA, it was already partially restored (53.3% of its normal level). Meanwhile, in contrast to the invisible change in GFAP level, expression of the neuron-specific marker proteins was abnormal in the MeCP2 shRNA group (Fig. 8D, E, H–O). These data indicate that astrocytes respond quickly to changes in the MeCP2 level, perhaps due to the spread of MeCP2-deficiency between astrocytes [36]. Given that a reduction of MeCP2 leads to slower astrocytic proliferation and weaker GFAP immunoreactivity [11, 36], the decreased GFAP expression at P14 may have resulted from disturbed astrocyte growth after MeCP2 knockdown. The restored expression of GFAP at P30 was probably a consequence of the partial restoration of MeCP2 expression in the P30 cerebellum and/or compensatory mechanisms for astrocytic growth in the mature brain. Notably, a previous study reported increased GFAP expression at 6 h after MeCP2 siRNA injection in the P2 female rat brain. The divergence of GFAP changes may be due to the time point for the assessment of GFAP level as well as gender [42]. On the other hand, however, neurons seemed to be insensitive to MeCP2 reduction at P14, but became abnormal by P30 when the MeCP2 expression had slightly recovered. The delay in the effect of MeCP2 knockdown on neurons implies a time threshold for neurons to respond to MeCP2 changes, similar to the findings reported by Nguyen *et al.* [24]. Considering that the MeCP2 expression was partially recovered at P30 in the MeCP2 shRNA group, together with its predominant distribution in neurons and enhanced expression at P30 (Figs. 2, 4, 7), there was probably a greater accumulation of neuronal MeCP2 from P14 to P30 in the MeCP2 shRNA group than in the control group. Therefore, the dramatic increase of MAP-2 as well as the reduction of DCX and Tuj1 at P30 may have resulted from the potential overexpression of neuronal MeCP2 in this period, as previously reported [43–47]. Last but not least, we found that Purkinje cells were more lightly stained by CB in the MeCP2 shRNA group at P30. Together with the decreased immature neurons in the PCL (Fig. 8N, O), these data suggest that the development of Purkinje cells is disturbed by MeCP2 interference. As Purkinje cells play an essential role in motor functions, and their degeneration is associated with motor defects [48–50], abnormal Purkinje cells in the MeCP2-deficient cerebellum may contribute to the progression of motor deficits in RTT patients. Further investigations are needed to elucidate the role of Purkinje cells in RTT and the underlying mechanisms.

Taken together, our data provide the first evidence that the patterns of expression and distribution of MeCP2 and diverse pMeCP2s are distinct and vary with the development of the rat brain. Moreover, MeCP2 and pS80 MeCP2 are concentrated in the nucleus, while pS421 MeCP2 and pS292 MeCP2 are mainly localized in the cytoplasm. Furthermore, MeCP2 and the pMeCP2s are predominantly expressed in neurons, but are also detectable in astrocytes at a relatively low level. Finally, postnatal interference with endogenous MeCP2 leads to the abnormal expression of neural marker proteins in the cerebellum, suggesting aberrant development of cerebellar neural cells after MeCP2 deficiency. A better understanding of the expressive patterns and exact roles of MeCP2 and the pMeCP2s in different brain regions is still needed, and this will provide further insights into the pathogenesis of RTT.

Acknowledgements The authors sincerely thank Ya-Lin Huang, Ling-Mei Zhang and Shan-Zheng Yang (Shanghai Medical College, Fudan University) for their excellent technical assistance. This work was supported by a grant from the National Natural Science Foundation of China (81030020).

References

1. Chahrour M, Jung SY, Shaw C, Zhou X, Wong ST, Qin J, *et al.* MeCP2, a key contributor to neurological disease, activates and represses transcription. Science 2008, 320: 1224–1229.
2. Damen D, Heumann R. MeCP2 phosphorylation in the brain: from transcription to behavior. Biol Chem 2013, 394: 1595–1605.

3. Zhou Z, Hong EJ, Cohen S, Zhao WN, Ho HY, Schmidt L, *et al.* Brain-specific phosphorylation of MeCP2 regulates activity-dependent Bdnf transcription, dendritic growth, and spine maturation. Neuron 2006, 52: 255–269.
4. Tao J, Hu K, Chang Q, Wu H, Sherman NE, Martinowich K, *et al.* Phosphorylation of MeCP2 at Serine 80 regulates its chromatin association and neurological function. Proc Natl Acad Sci U S A 2009, 106: 4882–4887.
5. Li H, Zhong X, Chau KF, Williams EC, Chang Q. Loss of activity-induced phosphorylation of MeCP2 enhances synaptogenesis, LTP and spatial memory. Nat Neurosci 2011, 14: 1001–1008.
6. Cohen S, Gabel HW, Hemberg M, Hutchinson AN, Sadacca LA, Ebert DH, *et al.* Genome-wide activity-dependent MeCP2 phosphorylation regulates nervous system development and function. Neuron 2011, 72: 72–85.
7. Cheng TL, Qiu Z. MeCP2: multifaceted roles in gene regulation and neural development. Neurosci Bull 2014, 30: 601–609.
8. Liu F, Ni JJ, Huang JJ, Kou ZW, Sun FY. VEGF overexpression enhances the accumulation of phospho-S292 MeCP2 in reactive astrocytes in the adult rat striatum following cerebral ischemia. Brain Res 2015, 1599: 32–43.
9. Gonzales ML, Adams S, Dunaway KW, LaSalle JM. Phosphorylation of distinct sites in MeCP2 modifies cofactor associations and the dynamics of transcriptional regulation. Mol Cell Biol 2012, 32: 2894–2903.
10. Mullaney BC, Johnston MV, Blue ME. Developmental expression of methyl-CpG binding protein 2 is dynamically regulated in the rodent brain. Neuroscience 2004, 123: 939–949.
11. Ballas N, Lioy DT, Grunseich C, Mandel G. Non-cell autonomous influence of MeCP2-deficient glia on neuronal dendritic morphology. Nat Neurosci 2009, 12: 311–317.
12. Maezawa I, Jin LW. Rett syndrome microglia damage dendrites and synapses by the elevated release of glutamate. J Neurosci 2010, 30: 5346–5356.
13. Miyake K, Nagai K. Phosphorylation of methyl-CpG binding protein 2 (MeCP2) regulates the intracellular localization during neuronal cell differentiation. Neurochem Int 2007, 50: 264–270.
14. Aber KM, Nori P, MacDonald SM, Bibat G, Jarrar MH, Kaufmann WE. Methyl-CpG-binding protein 2 is localized in the postsynaptic compartment: an immunochemical study of subcellular fractions. Neuroscience 2003, 116: 77–80.
15. Li X, Liu X, Guo H, Zhao Z, Li YS, Chen G. The significance of the increased expression of phosphorylated MeCP2 in the membranes from patients with proliferative diabetic retinopathy. Sci Rep 2016, 6: 32850.
16. Amir RE, Van den Veyver IB, Wan M, Tran CQ, Francke U, Zoghbi HY. Rett syndrome is caused by mutations in X-linked MECP2, encoding methyl-CpG-binding protein 2. Nat Genet 1999, 23: 185–188.
17. Hagberg B, Aicardi J, Dias K, Ramos O. A progressive syndrome of autism, dementia, ataxia, and loss of purposeful hand use in girls: Rett's syndrome: report of 35 cases. Ann Neurol 1983, 14: 471–479.
18. Bebbington A, Downs J, Percy A, Pineda M, Zeev BB, Bahi-Buisson N, *et al.* The phenotype associated with a large deletion on MECP2. Eur J Hum Genet 2012, 20: 921–927.
19. Jellinger K, Armstrong D, Zoghbi HY, Percy AK. Neuropathology of Rett syndrome. Acta Neuropathol 1988, 76: 142–158.
20. Na ES, Monteggia LM. The role of MeCP2 in CNS development and function. Horm Behav 2011, 59: 364–368.
21. Guy J, Hendrich B, Holmes M, Martin JE, Bird A. A mouse Mecp2-null mutation causes neurological symptoms that mimic Rett syndrome. Nat Genet 2001, 27: 322–326.
22. Collins AL, Levenson JM, Vilaythong AP, Richman R, Armstrong DL, Noebels JL, *et al.* Mild overexpression of MeCP2 causes a progressive neurological disorder in mice. Hum Mol Genet 2004, 13: 2679–2689.
23. Guy J, Gan J, Selfridge J, Cobb S, Bird A. Reversal of neurological defects in a mouse model of Rett syndrome. Science 2007, 315: 1143–1147.
24. Nguyen MV, Du F, Felice CA, Shan X, Nigam A, Mandel G, *et al.* MeCP2 is critical for maintaining mature neuronal networks and global brain anatomy during late stages of postnatal brain development and in the mature adult brain. J Neurosci 2012, 32: 10021–10034.
25. Cheval H, Guy J, Merusi C, De Sousa D, Selfridge J, Bird A. Postnatal inactivation reveals enhanced requirement for MeCP2 at distinct age windows. Hum Mol Genet 2012, 21: 3806–3814.
26. Tfilin M, Sudai E, Merenlender A, Gispan I, Yadid G, Turgeman G. Mesenchymal stem cells increase hippocampal neurogenesis and counteract depressive-like behavior. Mol Psychiatry 2009, 15: 1164–1175.
27. Petrov ES, Varlinskaya EI, Smotherman WP. The first suckling episode in the rat: the role of endogenous activity at mu and kappa opioid receptors. Dev Psychobiol 2000, 37: 129–143.
28. Song C, Feodorova Y, Guy J, Peichl L, Jost KL, Kimura H, *et al.* DNA methylation reader MECP2: cell type- and differentiation stage-specific protein distribution. Epigenetics Chromatin 2014, 7: 17.
29. Shahbazian MD, Antalffy B, Armstrong DL, Zoghbi HY. Insight into Rett syndrome: MeCP2 levels display tissue- and cell-specific differences and correlate with neuronal maturation. Hum Mol Genet 2002, 11: 115–124.
30. Mnatzakanian GN, Lohi H, Munteanu I, Alfred SE, Yamada T, MacLeod PJ, *et al.* A previously unidentified MECP2 open reading frame defines a new protein isoform relevant to Rett syndrome. Nat Genet 2004, 36: 339–341.
31. Jung BP, Jugloff DG, Zhang G, Logan R, Brown S, Eubanks JH. The expression of methyl CpG binding factor MeCP2 correlates with cellular differentiation in the developing rat brain and in cultured cells. J Neurobiol 2003, 55: 86–96.
32. Chen RZ, Akbarian S, Tudor M, Jaenisch R. Deficiency of methyl-CpG binding protein-2 in CNS neurons results in a Rett-like phenotype in mice. Nat Genet 2001, 27: 327–331.
33. Fyffe SL, Neul JL, Samaco RC, Chao HT, Ben-Shachar S, Moretti P, *et al.* Deletion of Mecp2 in Sim1-expressing neurons reveals a critical role for MeCP2 in feeding behavior, aggression, and the response to stress. Neuron 2008, 59: 947–958.
34. Samaco RC, Mandel-Brehm C, Chao HT, Ward CS, Fyffe-Maricich SL, Ren J, *et al.* Loss of MeCP2 in aminergic neurons causes cell-autonomous defects in neurotransmitter synthesis and specific behavioral abnormalities. Proc Natl Acad Sci U S A 2009, 106: 21966–21971.
35. Lioy DT, Garg SK, Monaghan CE, Raber J, Foust KD, Kaspar BK, *et al.* A role for glia in the progression of Rett's syndrome. Nature 2011, 475: 497–500.
36. Maezawa I, Swanberg S, Harvey D, LaSalle JM, Jin LW. Rett syndrome astrocytes are abnormal and spread MeCP2 deficiency through gap junctions. J Neurosci 2009, 29: 5051–5061.
37. Tsujimura K, Abematsu M, Kohyama J, Namihira M, Nakashima K. Neuronal differentiation of neural precursor cells is promoted by the methyl-CpG-binding protein MeCP2. Exp Neurol 2009, 219: 104–111.
38. Kishi N, Macklis JD. MECP2 is progressively expressed in post-migratory neurons and is involved in neuronal maturation rather than cell fate decisions. Mol Cell Neurosci 2004, 27: 306–321.
39. Shahbazian M, Young J, Yuva-Paylor L, Spencer C, Antalffy B, Noebels J, *et al.* Mice with truncated MeCP2 recapitulate many Rett syndrome features and display hyperacetylation of histone H3. Neuron 2002, 35: 243–254.

40. Cheval H, Guy J, Merusi C, De Sousa D, Selfridge J, Bird A. Postnatal Inactivation Reveals Enhanced Requirement for Mecp2 at Distinct Age Windows. Hum Mol Genet 2012, 21: 3806–3814.
41. McGraw CM, Samaco RC, Zoghbi HY. Adult neural function requires MeCP2. Science 2011, 333: 186.
42. Forbes-Lorman RM, Kurian JR, Auger AP. MeCP2 regulates GFAP expression within the developing brain. Brain Res 2014, 1543: 151–158.
43. Smrt RD, Eaves-Egenes J, Barkho BZ, Santistevan NJ, Zhao C, Aimone JB, *et al.* Mecp2 deficiency leads to delayed maturation and altered gene expression in hippocampal neurons. Neurobiol Dis 2007, 27: 77–89.
44. Rastegar M, Hotta A, Pasceri P, Makarem M, Cheung AY, Elliott S, *et al.* MECP2 isoform-specific vectors with regulated expression for Rett syndrome gene therapy. PLoS One 2009, 4: e6810.
45. Petazzi P, Akizu N, Garcia A, Estaras C, Martinez de Paz A, Rodriguez-Paredes M, *et al.* An increase in MECP2 dosage impairs neural tube formation. Neurobiol Dis 2014, 67: 49–56.
46. Cobb S, Guy J, Bird A. Reversibility of functional deficits in experimental models of Rett syndrome. Biochem Soc Trans 2010, 38: 498–506.
47. Marshak S, Meynard MM, De Vries YA, Kidane AH, Cohen-Cory S. Cell-autonomous alterations in dendritic arbor morphology and connectivity induced by overexpression of MeCP2 in Xenopus central neurons in vivo. PLoS One 2012, 7: e33153.
48. Ito M. Historical review of the significance of the cerebellum and the role of Purkinje cells in motor learning. Ann N Y Acad Sci 2002, 978: 273–288.
49. Millen KJ, Gleeson JG. Cerebellar development and disease. Curr Opin Neurobiol 2008, 18: 12–19.
50. Koeppen AH. The pathogenesis of spinocerebellar ataxia. Cerebellum 2005, 4: 62–73.